Electronic Supplementary Information

Electrochemical CO_2 Reduction to Methane with Remarkably High Faradaic Efficiency in the Presence of a Proton Permeable Membrane

Hanqing Pan[a] and Christopher J. Barile[a*]

[a] Department of Chemistry, University of Nevada, Reno

*E-mail: cbarile@unr.edu

Table of Contents

Experimental

Materials and electrode preparation.

Nafion D520 dispersion and carbon paper (AvCarb EP40T) were purchased from Fuel Cell Store. Cu foil (99.99% purity) was purchased from All-Foils, Inc, Ni foil (99.9% purity) was purchased from Goodfellow, Inc., and Zn foil (99.99% purity) was purchased from Belmont Metals. Sodium bicarbonate was purchased from Sigma Aldrich. CO_2 and CO were purchased from Airgas. Nafion-modified electrodes were fabricated by drop-casting the Nafion dispersion directly onto the substrate.

Electrochemical Measurements and Material Characterization.

All electrochemical measurements were performed using a VSP-300 Biologic Potentiostat. All electrochemical data were collected versus a Ag/AgCl reference electrode and converted to the reversible hydrogen electrode (RHE) scale by $V_{(vs.\ RHE)} = V_{(measured\ vs.\ Ag/AgCl)} + 0.21 + 0.059*6.8$ (where 6.8 is the pH of solution). All values are reported versus RHE. Current densities are reported with respect to geometric area of the working electrode. For linear sweep voltammogram studies, the geometric working electrode area was 0.218 cm^2 and for all other experiments, the geometric working electrode area was 5.0 cm^2. To evaluate the CO_2 reduction activity of the thin films, the working electrodes were studied in 0.1 M sodium bicarbonate buffer sparged with CO_2 gas for at least 30 min using a one-compartment, three-electrode configuration. The thin films on carbon paper served as the working electrode, a Pt wire was used as the counter electrode, and a Ag/AgCl electrode was used as the reference electrode. Electrochemical impedance spectroscopy (EIS) was performed in 0.1 M sodium bicarbonate buffer sparged with CO_2 gas using a three-electrode configuration cell at -0.89 V vs. RHE. The frequency was varied from 200 kHz to 100 mHz sinusoidally with an amplitude of 10 mV. Scanning electron microscope (SEM) images and

energy-dispersive X-ray (EDS) analysis were obtained for each sample using a JEOL JSM-6010LA analytical SEM or a JEOL JSM-7100F field emission SEM operated using an accelerating voltage of 15 kV. Onset potentials were calculated by determining the voltage at which the current density reached 15% of the maximum current density for each linear sweep voltammogram.

Product Determination. Electrochemical reactions were performed chronoamperometrically at -0.89 V vs. RHE (and at -0.38 V, -0.13 V, and 0.12 V vs. RHE for voltage-dependent experiments) for one hour unless otherwise noted using carbon as a counter electrode in a beaker for determining liquid and solid products and Pt wire as a counter electrode in a custom-made cell for determining gas products (Figure S3). During chronoamperometry, CO_2 was continuously sparged through the solution (2.5 mL) at a rate of 5 cm^3/min. Liquid products were quantified using a Varian 400 MHz NMR Spectrometer using DMF as an internal standard. The water in the reaction solution was evaporated under reduced pressure, and sodium formate along with other residual solids from the electrolyte were collected and dissolved in D_2O. Liquid products were extracted from the reaction solution using deuterated chloroform. Gas products were quantified using a SRI 8610C gas chromatograph equipped with a flame ionization detector (FID) and a methanizer. The limits of detection for formate, liquid products, and gas products were determined to be 11 μM, 85 μM, and 1 ppm, respectively. All experiments were at least duplicated, and all error bars presented are the standard deviation among the multiple trials.

Calculations

Effect of Mass Transport on LSV Onset Potential with PVDF-modified Electrodes

The permeability of CO_2 in PVDF was taken to be 2.16 x 10^{-17} mol-cm/cm^2-s-Pa, a value obtained from Flaconneche *et al*.[38] Because the thickness of the PVDF membrane is 15 μm and the pressure of CO_2 is 1 atm, the flux of CO_2 through the membrane is calculated to be 1.5 x 10^{-9} mol/cm^2-s. This flux value is then compared to the maximum theoretical rate of consumption of CO_2 at the electrode-polymer interface. The maximum CO_2 consumption rate is determined from the current density of the LSV, assuming all CO_2 is reduced to either CO or HCOOH. Because these products require only 2 e^-/mol, they consume CO_2 faster than more highly reduced products such as CH_4. Therefore, assuming a 100% yield of CO or HCOOH is an upper bound for the CO_2 consumption rate. For the PVDF-covered Cu electrode, the current density at the onset potential (-0.55 V) of the LSV is -0.26 mA/cm^2. From this value, the upper bound for the CO_2 consumption rate is 1.3 x 10^{-9} mol/cm^2-s, a value less than the calculated CO_2 flux. Therefore, these calculations suggest that CO_2 mass transport is not a limiting factor during the onset potential region of the LSVs with 15 μm PVDF overlayers.

Effect of Mass Transport on CO_2 Electrocatalysis on Nafion-modified Electrodes

The permeability of CO_2 in Nafion was taken to be 8.70 x 10^{-16} mol-cm/cm^2-s-Pa, a value obtained from Ren *et al*.[39] With a 15 μm Nafion overlayer, the flux of CO_2 is calculated to be 5.9 x 10^{-8} mol/cm^2-s. The steady state current of the chronoamperometry of this electrode is about -0.5 mA/cm^2. From this current density, we use the protocol described in the above paragraph to determine that the maximum theoretical CO_2 consumption rate at the electrode-polymer interface is 2.6 x 10^{-9} mol/cm^2-s. In other words, the maximum CO_2 consumption rate is more than an order of magnitude less than CO_2 flux through Nafion. These calculations indicate that CO_2 electrocatalysis is not limited by CO_2 availability at the electrode-polymer interface with a 15 μm Nafion overlayer. Analogous calculations with a 183 μm Nafion overlayer give a calculated CO_2 flux of 4.8 x 10^{-9} mol/cm^2-s, a value much closer to the maximum CO_2 consumption rate.

Effect of Electrical Conductivity of Nafion on Voltammetry

Given that the bulk electrical conductivity of Nafion is less than 10^{-4} S/cm,[40] and that the maximum current density of the LSV of the Cu electrode with a 15 μm Nafion layer in Fig. 1B is -3.5 mA/cm^2, the calculated voltage drop due to resistance across a 15 μm Nafion layer is greater than 50 mV, a value large enough to give rise to changes in the shape of the voltammogram.

Percent Conversion of CO_2

As noted in the experimental section, the reaction vessel was continuously sparged at a rate of 5 cm^3/min with CO_2 during chronoamperometry. The number of moles of electrons consumed during catalysis is much less than the number of moles of CO_2 passed through the electrochemical cell. For the case of the electrode with the highest CH_4 Faradaic efficiency (88%), we calculate that the total CO_2 conversion yield is 0.1%. In an industrial application, this low conversion yield could be improved by optimizing the CO_2 flow rate and electrode porosity as well as by using multiple passes of the same CO_2 reactant stream.

Supplementary Figures

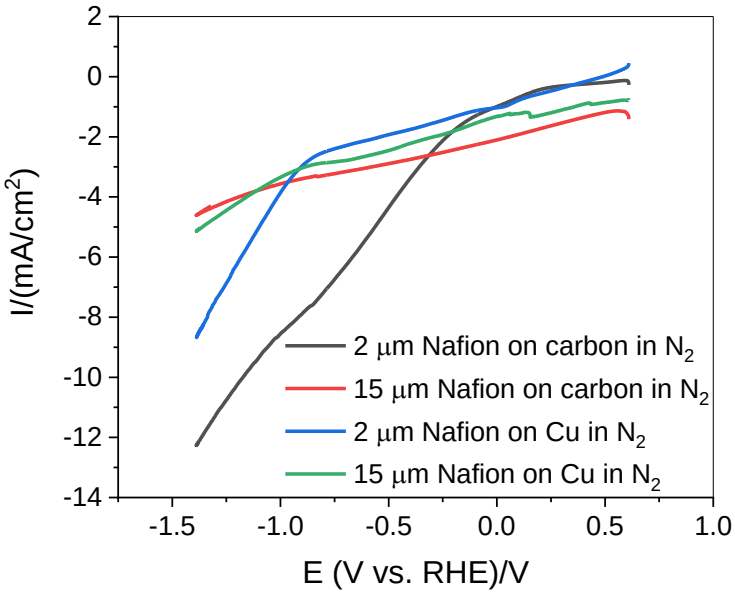

Figure S1. Linear sweep voltammograms of carbon and Cu foil modified with 2 µm (grey, blue lines) and 15 µm (red, green lines) Nafion overlayers in N_2-saturated 0.1 M $NaHCO_3$ electrolyte at a scan rate of 10 mV/s.

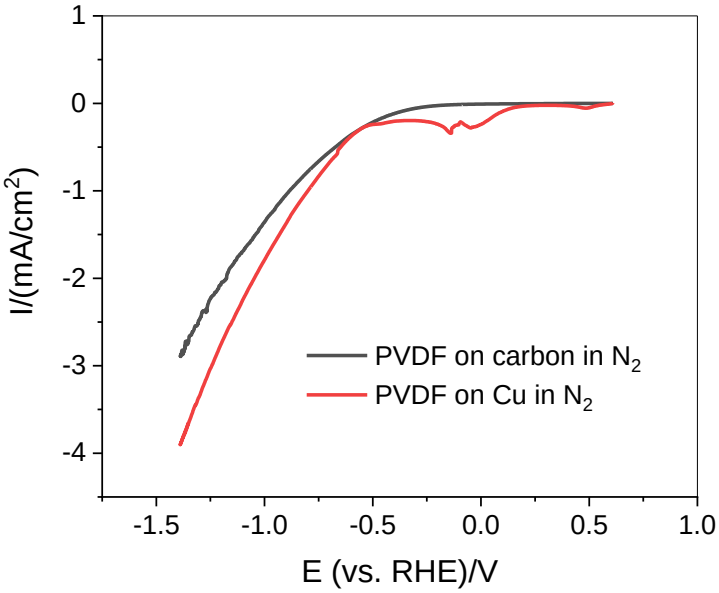

Figure S2. Linear sweep voltammograms of PVDF-modified carbon and Cu foil in N_2-saturated 0.1 M $NaHCO_3$ electrolyte at a scan rate of 10 mV/s.

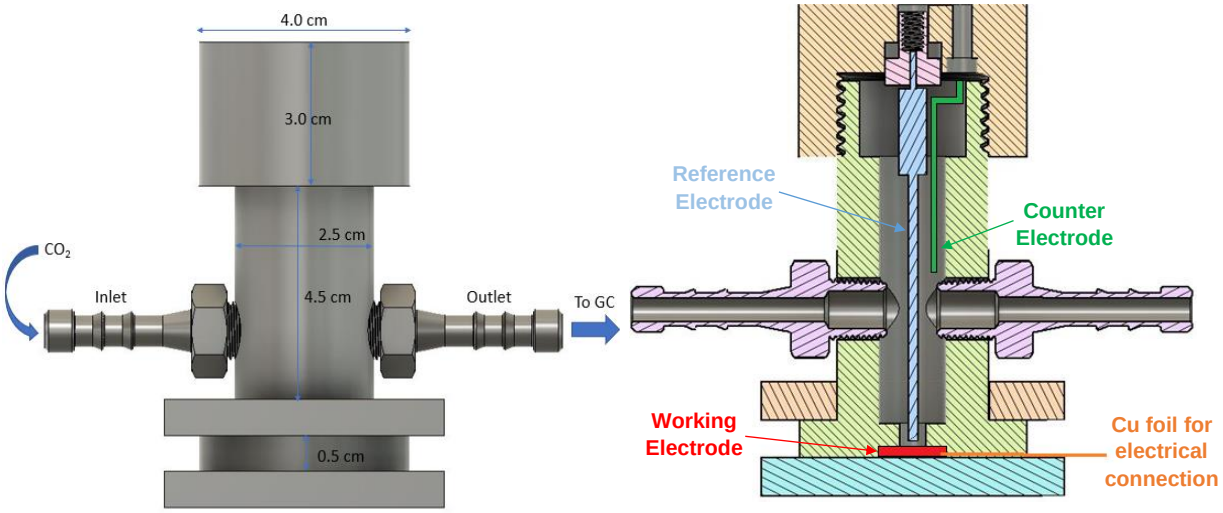

Figure S3. Schematics of custom-made cell for gas collection. The size of the working electrode was 5.0 cm^2, and the length of the 1.0 mm diameter Pt wire counter electrode was 3.0 cm. The reference and counter were 0.5 cm away from each other and 0.5 cm away from the working electrode. The reference and counter electrodes were positioned through o-ring sealed ports on the top of the cell. The working electrode was placed on the bottom of the cell and was hermetically sealed using a compressed o-ring. The figure on the right highlights the positions of the three electrodes. The volume of solution used for electrocatalysis was 2.5 mL. Gas products were purged from the cell by a 20 mL glass syringe and sent to the GC for analysis.

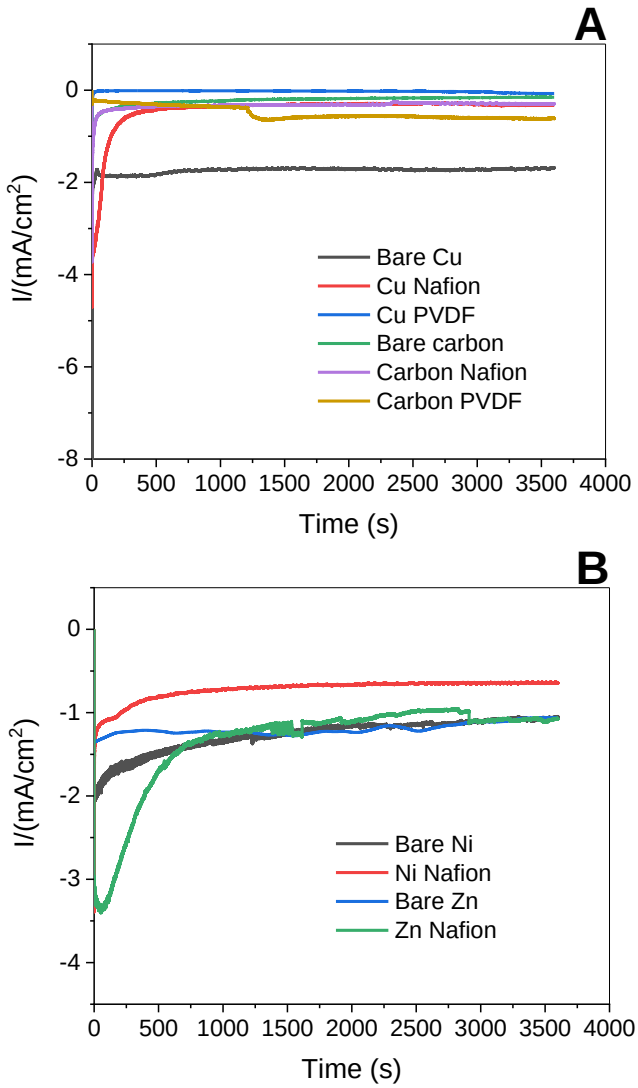

Figure S4. Chronoamperometry curves over 1 hr of electrochemical CO_2 reduction using bare, Nafion-modified, and PVDF-modified carbon and Cu electrodes (A) and bare and Nafion-modified Ni and Zn electrodes (B).

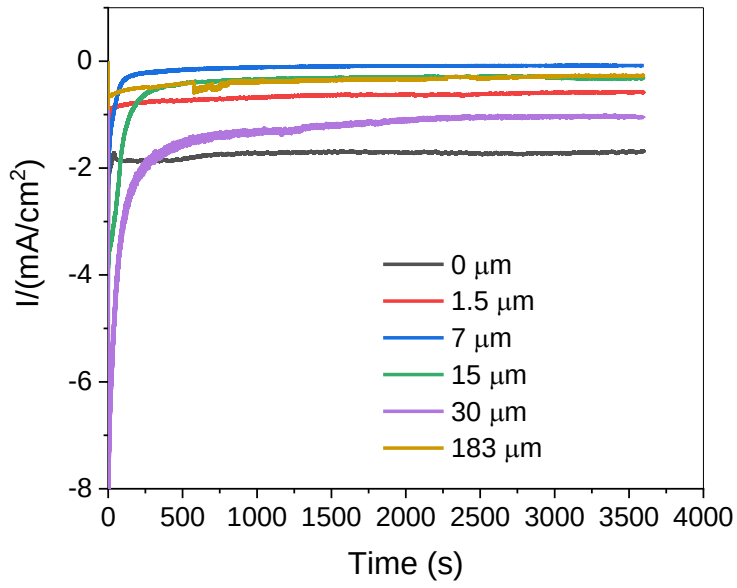

Figure S5. Chronoamperometry curves over 1 hr of electrochemical CO_2 reduction using varying thicknesses of Nafion overlayer on Cu electrodes.

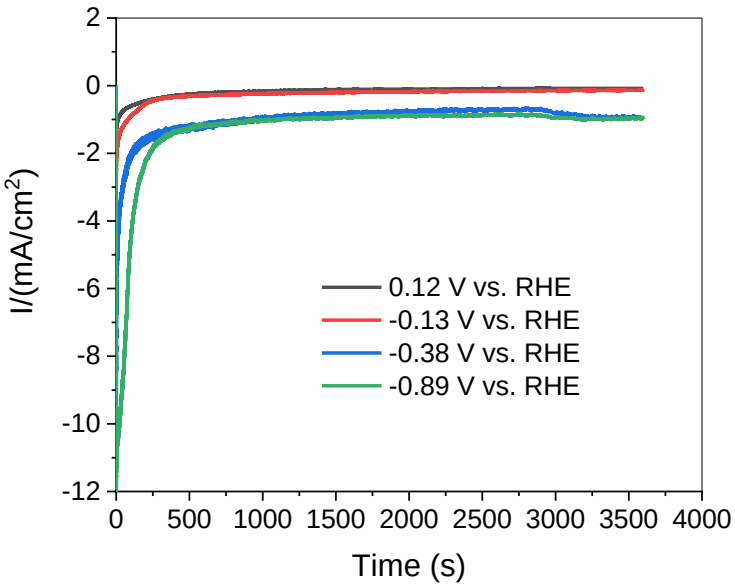

Figure S6. Chronoamperometry curves over 1 hr of electrochemical CO_2 reduction using Cu electrode modified with 15 μm of Nafion at various voltages.

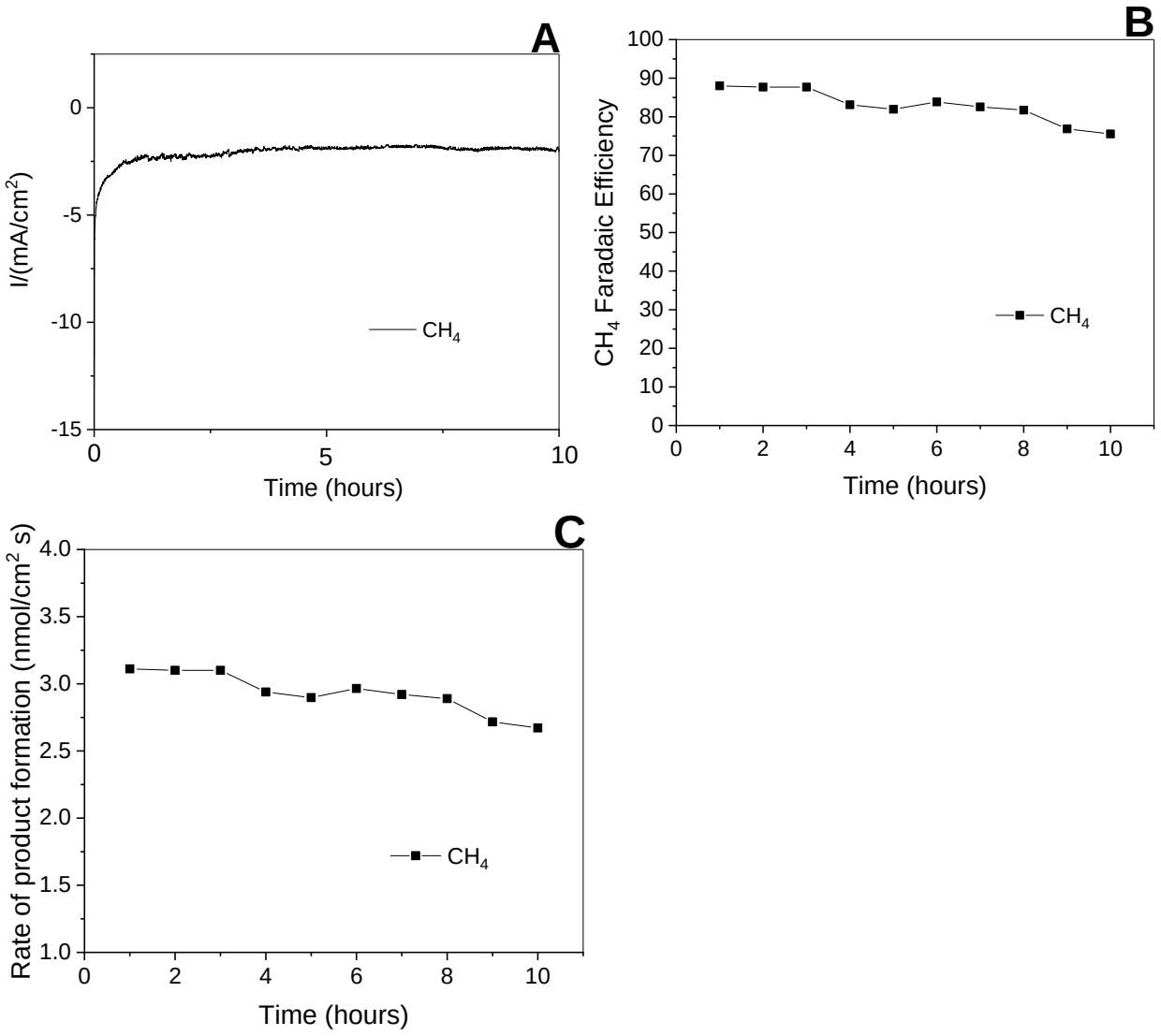

Figure S7. Chronoamperometry (A), Faradaic efficiency (B), and rate (C) of CH_4 production over 10 hours at -0.38 V vs. RHE using a Cu electrode modified with 15 µm Nafion overlayer.

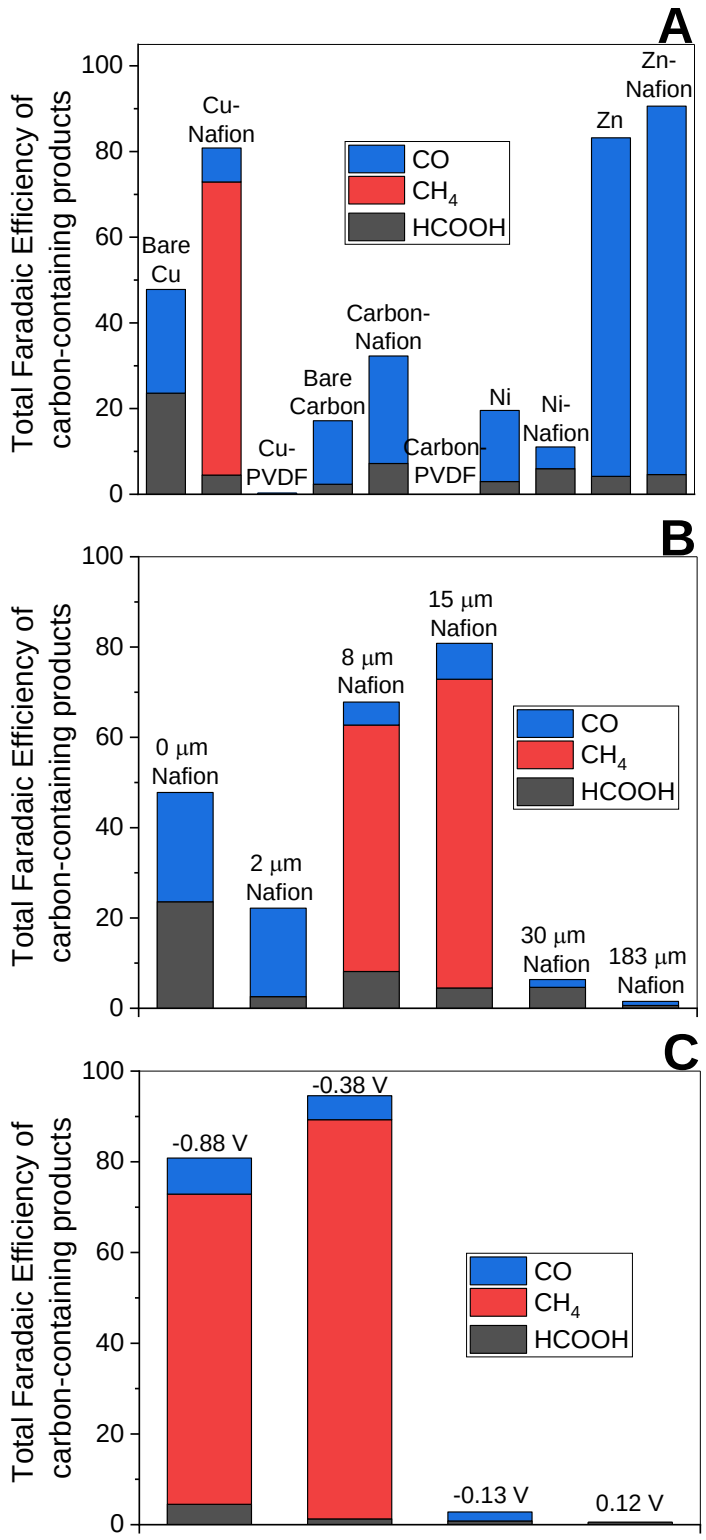

Figure S8. Total Faradaic efficiencies of carbon-containing products obtained from bare electrodes and electrodes modified with 15 μm of Nafion or PVDF (A), varying the thickness of Nafion overlayer on Cu electrode (B), and varying the voltage of the electrochemical reaction (C).

Table S1. R^2 values obtained from linear sweep voltammograms fitted with a linear trend line.

Electrode	R^2 value
Bare carbon	0.853
Carbon with 2 µm Nafion	0.898
Carbon with 15 µm Nafion	0.997
Bare Cu	0.871
Cu with 2 µm Nafion	0.939
Cu with 15 µm Nafion	0.969

Table S2. Faradaic efficiencies for CO, CH_4, and HCOOH for all catalysts at -0.89 V vs. RHE on bare substrates, 15 µm Nafion-modified substrates, and 15 µm PVDF-modified substrates.

Substrate	CO Faradaic Efficiency (%)	CH_4 Faradaic Efficiency (%)	HCOOH Faradaic Efficiency (%)
Bare Cu	24.2 ± 3	0	23.6 ± 4
Cu-Nafion	7.94 ± 1	68.4 ± 17	4.49 ± 0.8
Cu-PVDF	0.28 ± 0.03	0	0
Bare carbon	14.8 ± 2	0	2.36 ± 0.4
Carbon-Nafion	25.1 ± 3.5	0	7.19 ± 1.2
Carbon-PVDF	0	0	0
Ni	16.6 ± 2	0	2.97 ± 0.5
Ni-Nafion	5.07 ± 0.7	0	5.97 ± 1
Zn	79 ± 10	0	4.2 ± 0.7
Zn-Nafion	86 ± 11	0	4.6 ± 0.7

Table S3. Summary of various electrocatalysts for electrochemical CO_2 reduction to CH_4 reported in literature.

Catalyst	Voltage (vs. RHE)	Electrolyte	CH_4 Faradaic Efficiency (%)	Reference
Cu foil	-2.4 V	$NaClO_4$/MeOH	70.5	[1]
Cu-Co electrode	-1.19 V	0.1 M $KHCO_3$	47.5	[2]
Cu foil	-1.2 V	0.1 M $KHCO_3$	40	[3]
Cu electrode	-1.04 V	0.1 M $KHCO_3$	33.3	[4]
Pd electrode	-0.80 V	0.1 M $KHCO_3$	2.9	[4]
Cd electrode	-1.23 V	0.1 M $KHCO_3$	1.3	[4]
Ni electrode	-1.08 V	0.1 M $KHCO_3$	1.8	[4]
N-doped graphene quantum dots	-0.86 V	1 M KOH	15	[5]
Ti-phthalocyanine	-1.58 V	--	28.1	[6]
Cu-phthalocyanine	-1.23 V	--	28.0	[6]
Cu nanofoam	-1.5 V	0.1 M $KHCO_3$	< 2	[7]
Pt GDE	-1.32 V	0.5 M $KHCO_3$	38.8	[8]
Pt/C	0.0 V	--	6.8	[9]
Cu single crystal	-1.01 V	0.1 M $KHCO_3$	6	[10]
Cu mesh	-1.2 V	2 M KBr	28.8	[11]
Cu nanocubes (24 nm)	-1.1 V	0.1 M $KHCO_3$	15	[12]
Cu nanocubes (44 nm)	-1.1 V	0.1 M $KHCO_3$	22	[12]
Cu nanocubes (63 nm)	-1.1 V	0.1 M $KHCO_3$	10	[12]
Cu foil	-1.1 V	0.1 M $KHCO_3$	18	[12]
Polycrystalline Cu	-1.0 V	0.1 M $KHCO_3$	4.6	[13]
Cu nanoparticles	-1.35 V	0.1 M $NaHCO_3$	76	[14]
Cu_2O/Zn	-1.9 V	0.3 M KOH in MeOH	7.5	[15]
Nanoporous carbon	-1.6 V	0.1 M $KHCO_3$	0.18	[16]
Cu electrode	-1.05 V	0.1 M $LiHCO_3$	32.2	[17]
Cu electrode	-1.05 V	0.1 M $NaHCO_3$	55.1	[17]
Cu electrode	-0.99 V	0.1 M $KHCO_3$	32.0	[17]
Cu electrode	-0.98 V	0.1 M $CsHCO_3$	16.3	[17]
Cu_2O films	-1.1 V	0.1 M $KHCO_3$	5	[18]
Cu_2O films	-0.99 V	0.1 M $KHCO_3$	< 1	[19]
Cu electrode	-1.01 V	0.1 M $KHCO_3$	29.4	[20]
Cu electrode	-1.04 V	0.1 M KCl	11.5	[20]
Cu electrode	-0.99 V	0.5 M KCl	14.5	[20]
Cu electrode	-1.00 V	0.1 M $KClO_4$	10.2	[20]
Cu electrode	-1.00 V	0.1M K_2SO_4	12.3	[20]
Cu electrode	-0.83 V	0.5 M K_2HPO_4	17.0	[20]
Cu electrode	-0.77 V	0.1 M K_2HPO_4	6.6	[20]
Cu electrode	-0.96 V	0.1 M $KHCO_3$	22.3	[21]
Fe electrode	-0.98 V	0.1 M $KHCO_3$	1.1	[21]
Ni electrode	-1.09 V	0.1 M $KHCO_3$	1.1	[21]

Cu electrode	-1.0 V	0.1 M $KHCO_3$	3	[22]
Cu-Ni electrode	-1.3 V	0.5 M $KHCO_3$	20.2	[23]
Ag electrode	-1.4 V	0.1 M $KHCO_3$	0.09	[24]
Ni electrode	-1.00 V	0.1 M $KHCO_3$	0.6	[25]
Ni electrode	-1.08 V	0.1 M $KHCO_3$	1.8	[25]
Ni electrode	-1.02 V	0.1 M $KHCO_3$	2.4	[25]
Cu sheet	-1.00 V	0.1 M $KHCO_3$	16.3	[26]
Cu_2O/carbon black	-1.3 V	NaCl/MeOH	26.9	[27]
Cu sheet	-1.35 V	0.1 M $KHCO_3$	44	[28]
Cu porphyrin	-1.0 V	0.5 M $KHCO_3$	26	[29]
Cu electrode	-1.35 V	0.5 M $KHCO_3$	5.3	[30]
Cu electrode	-1.6 V	1.1 M $KHCO_3$	44	[31]
Cu electrode	-2.4 V	0.5 M $LiClO_4$/MeOH	71.8	[32]
Cu wire electrode	-3.35 V	Tetraethylammonium perchlorate methanol	28.1	[33]
Cu nanoparticles	-1.3 V	0.1 M $KHCO_3$	50	[34]
Cu_2Pd	-1.2 V	0.1 M $TBAPF_6/CH_3CN$	55	[35]
Co protoporphyrin	-0.8 V	0.1 M $HClO_4$	2.5	[36]
Polycrystalline Cu	-1.4 V	0.5 M $KHCO_3$	42	[37]

References

1. S. Kaneco, H. Katsumata, T. Suzuki and K. Ohta, Electrochemical Reduction of CO_2 to Methane at the Cu Electrode in Methanol with Sodium Supporting Salts and Its Comparison with Other Alkaline Salts. *Energy Fuels*, 2006, **20** (1), 409-414.
2. Y. Takatsuji, I. Nakata, M. Morimoto, T. Sakakura, R. Yamasaki and T. Haruyama, Highly Selective Methane Production Through Electrochemical CO_2 reduction by Electrolytically Plated Cu-Co Electrode. *Electrocatalysis*, 2019, **10** (1), 29-34.
3. K. P. Kuhl, E. R. Cave, D. N. Abram and T. F. Jaramillo, New insights into the electrochemical reduction of carbon dioxide on metallic copper surfaces. *Energy Environ. Sci.,* 2012, **5** (5), 7050-7059.
4. Y. Hori, H. Wakebe, T. Tsukamoto and O. Koga, Electrocatalytic process of CO selectivity in electrochemical reduction of CO_2 at metal electrodes in aqueous media. *Electrochim. Acta,* 1994, **39** (11), 1833-1839.
5. J. Wu, S. Ma, J. Sun, J. I. Gold, C. Tiwary, B. Kim, L. Zhu, N. Chopra, I. N. Odeh, R. Vajtai, A. Z. Yu, R. Luo, J. Lou, G. Ding, P. J. A. Kenis and P. M. Ajayan, A metal-free electrocatalyst for carbon dioxide reduction to multi-carbon hydrocarbons and oxygenates. *Nat. Commun.,* 2016, **7** (1), 13869.
6. N. Furuya and S. Koide, Electroreduction of carbon dioxide by metal phthalocyanines. *Electrochim. Acta,* 1991, **36** (8), 1309-1313.
7. S. Sen, D. Liu and G. T. R. Palmore, Electrochemical Reduction of CO_2 at Copper Nanofoams. *ACS Catal.*, 2014, **4** (9), 3091-3095.
8. K. Hara, Electrocatalytic Formation of CH_4 from CO_2 on a Pt Gas Diffusion Electrode. *J. Electrochem. Soc.*, 1997, **144** (2), 539.
9. M. Umeda, Y. Niitsuma, T. Horikawa, S. Matsuda and M. Osawa, Electrochemical Reduction of CO_2 to Methane on Platinum Catalysts without Overpotentials: Strategies for Improving Conversion Efficiency. *ACS Appl. Energy Mater.*, 2020, **3** (1), 1119-1127.
10. I. Takahashi, O. Koga, N. Hoshi and Y. Hori, Electrochemical reduction of CO_2 at copper single crystal Cu(S)-[n(111)×(111)] and Cu(S)-[n(110)×(100)] electrodes. *J. Electroanal. Chem.,* 2002, **533** (1), 135-143.
11. H. Yano, T. Tanaka, M. Nakayama and K. Ogura, Selective electrochemical reduction of CO_2 to ethylene at a three-phase interface on copper(I) halide-confined Cu-mesh electrodes in acidic solutions of potassium halides. *J. Electroanal. Chem.*, 2004, **565** (2), 287-293.
12. A. Loiudice, P. Lobaccaro, E. A. Kamali, T. Thao, B. H. Huang, J. W. Ager and R. Buonsanti, Tailoring Copper Nanocrystals towards C2 Products in Electrochemical CO_2 Reduction. *Angew. Chem. Int. Ed.*, 2016, **55** (19), 5789-5792.
13. Y. Kwon, Y. Lum, E. L. Clark, J. W. Ager and A. T. Bell, CO_2 Electroreduction with Enhanced Ethylene and Ethanol Selectivity by Nanostructuring Polycrystalline Copper. *ChemElectroChem*, 2016, **3** (6), 1012-1019.
14. K. Manthiram, B. J. Beberwyck and A. P. Alivisatos, Enhanced Electrochemical Methanation of Carbon Dioxide with a Dispersible Nanoscale Copper Catalyst. *J. Am. Chem. Soc.*, 2014, **136** (38), 13319-13325.
15. S. Ohya, S. Kaneco, H. Katsumata, T. Suzuki and K. Ohta, Electrochemical reduction of CO_2 in methanol with aid of CuO and Cu_2O. *Catal.*, 2009, **148** (3), 329-334.
16. W. Li, M. Seredych, E. Rodríguez-Castellón and T. J. Bandosz, Metal-free Nanoporous Carbon as a Catalyst for Electrochemical Reduction of CO_2 to CO and CH_4. *ChemSusChem*, 2016, **9** (6), 606-616.

17. A. Murata and Y. Hori, Product Selectivity Affected by Cationic Species in Electrochemical Reduction of CO_2 and CO at a Cu Electrode. *Bull. Chem. Soc. Jpn.*, 1991, **64** (1), 123-127.
18. R. Kas, R. Kortlever, A. Milbrat, M. T. M. Koper, G. Mul and J. Baltrusaitis, Electrochemical CO_2 reduction on Cu_2O-derived copper nanoparticles: controlling the catalytic selectivity of hydrocarbons. *Phys. Chem. Chem. Phys.*, 2014, **16** (24), 12194-12201.
19. D. Ren, Y. Deng, A. D. Handoko, C. S. Chen, S. Malkhandi and B. S. Yeo, Selective Electrochemical Reduction of Carbon Dioxide to Ethylene and Ethanol on Copper(I) Oxide Catalysts. *ACS Catal.* 2015, **5** (5), 2814-2821.
20. Y. Hori, A. Murata and R. Takahashi, Formation of hydrocarbons in the electrochemical reduction of carbon dioxide at a copper electrode in aqueous solution. *J. Chem. Soc. Faraday Trans.*, 1989**, 85** (8), 2309-2326.
21. Y. Hori, R. Takahashi, Y. Yoshinami and A. Murata, Electrochemical Reduction of CO at a Copper Electrode. *J. Phys. Chem. B*, 1997, **101** (36), 7075-7081.
22. Y. Lum, B. Yue, P. Lobaccaro, A. T. Bell and J. W. Ager, Optimizing C–C Coupling on Oxide-Derived Copper Catalysts for Electrochemical CO_2 Reduction. *J. Phys. Chem. C*, 2017, **121** (26), 14191-14203.
23. S. S. Y. Kaneco, H. Katsumata, T. Suzuki and K. Ohta, Cu-deposited Nickel Electrode for the Electrochemical Conversion of CO_2 in Water/methanol Mixture Media. *Bull. Catal. Soc. India*, 2007, **6**, 71-82.
24. T. Hatsukade, K. P. Kuhl, E. R. Cave, D. N. Abram and T. F. Jaramillo, Insights into the electrocatalytic reduction of CO_2 on metallic silver surfaces. *Phys. Chem. Chem. Phys.*, 2014, **16** (27), 13814-13819.
25. Y. Hori and A. Murata, Electrochemical evidence of intermediate formation of adsorbed CO in cathodic reduction of CO_2 at a nickel electrode. *Electrochim. Acta*, 1990, **35** (11), 1777-1780.
26. Y. Hori, A. Murata, R. Takahashi and S. Suzuki, Electroreduction of carbon monoxide to methane and ethylene at a copper electrode in aqueous solutions at ambient temperature and pressure. *J. Am. Chem. Soc.*, 1987, **109** (16), 5022-5023.
27. N. Uemoto, M. Furukawa, I. Tateishi, H. Katsumata and S. Kaneco, Electrochemical Carbon Dioxide Reduction in Methanol at Cu and Cu_2O-Deposited Carbon Black Electrodes. *ChemEngineering*, 2019, **3** (1), 1-10.
28. A. Engelbrecht, C. Uhlig, O. Stark, M. Hämmerle, G. Schmid, E. Magori, K. Wiesner-Fleischer, M. Fleischer and R. Moos, On the Electrochemical CO_2 Reduction at Copper Sheet Electrodes with Enhanced Long-Term Stability by Pulsed Electrolysis. *J. Electrochem. Soc.*, 2018, **165** (15), J3059-J3068.
29. Z. Weng, J. Jiang, Y. Wu, Z. Wu, X. Guo, K. L. Materna, W. Liu, V. S. Batista, G. W. Brudvig and H. Wang, Electrochemical CO_2 Reduction to Hydrocarbons on a Heterogeneous Molecular Cu Catalyst in Aqueous Solution. *J. Am. Chem. Soc.*, 2016, **138** (26), 8076-8079.
30. D. W. Dewulf and A. J. Bard, The electrochemical reduction of CO_2 to CH_4 and C_2H_4 at Cu/Nafion electrodes (solid polymer electrolyte structures). *Catal. Lett.*, 1988, **1** (1), 73-79.
31. S. Kaneco, N.-h. Hiei, Y. Xing, H. Katsumata, H. Ohnishi, T. Suzuki and K. Ohta, High-efficiency electrochemical CO_2-to-methane reduction method using aqueous $KHCO_3$ media at less than 273 K. *J. Solid State Electr.*, 2003, **7** (3), 152-156.
32. S. Kaneco, K. Iiba, M. Yabuuchi, N. Nishio, H. Ohnishi, H. Katsumata, T. Suzuki and K. Ohta, High Efficiency Electrochemical CO_2-to-Methane Conversion Method Using Methanol with Lithium Supporting Electrolytes. *Ind. Eng. Chem. Res.*, 2002, **41** (21), 5165-5170.

33. S. Kaneco, K. Iiba, K. Ohta and T. Mizuno, Electrochemical CO_2 Reduction on a Copper Wire Electrode in Tetraethylammonium Perchlorate Methanol at Extremely Low Temperature. *Energy Sources,* 1999, **21** (7), 643-648.
34. M. K. Kim, H. J. Kim, H. Lim, Y. Kwon and H. M. Jeong, Metal–organic framework-mediated strategy for enhanced methane production on copper nanoparticles in electrochemical CO_2 reduction. *Electrochim. Acta,* 2019, **306**, 28-34.
35. S. Zhang, P. Kang, M. Bakir, A. M. Lapides, C. J. Dares and T. J. Meyer, Polymer-supported CuPd nanoalloy as a synergistic catalyst for electrocatalytic reduction of carbon dioxide to methane. *Proc. Natl. Acad. Sci.,* 2015, **112** (52), 15809.
36. J. Shen, R. Kortlever, R. Kas, Y. Y. Birdja, O. Diaz-Morales, Y. Kwon, I. Ledezma-Yanez, K. J. P. Schouten, G. Mul and M. T. M. Koper, Electrocatalytic reduction of carbon dioxide to carbon monoxide and methane at an immobilized cobalt protoporphyrin. *Nat. Commun.,* 2015, **6** (1), 8177.
37. H. Hashiba, H. K. Sato, S. Yotsuhashi, K. Fujii, M. Sugiyama and Y. Nakano, A broad parameter range for selective methane production with bicarbonate solution in electrochemical CO_2 reduction. *Sustain. Energy Fuels,* 2017, **1** (8), 1734-1739.
38. B. Flaconneche, J. Martin and M. H. Klopffer, Permeability, Diffusion and Solubility of Gases in Polyethylene, Polyamide 11 and Poly (Vinylidene Fluoride). *Oil Gas Sci. Technol. - Rev. IFP*, 2001, **56** (3), 261-278.
39. X. Ren, T. D. Myles, K. N. Grew and W. K. S. Chiu, Carbon Dioxide Transport in Nafion 1100 EW Membrane and in a Direct Methanol Fuel Cell. *J. Electrochem. Soc.,* 2015, **162** (10), F1221-F1230.
40. N. P. Cele and S. S. Ray, Effect of Multiwalled Carbon Nanotube Loading on the Properties of Nafion Membranes. *J. Mater. Res.*, 2015, **30** (1), 66-78.